Role of coherence in quantum-dot-based nanomachines within the Coulomb blockade regime

Federico D. Ribetto,[1,2] Raúl A. Bustos-Marún,[1,3,*] and Hernán L. Calvo[1,2]
[1]*Instituto de Física Enrique Gaviola (CONICET) and FaMAF, Universidad Nacional de Córdoba, Argentina*
[2]*Departamento de Física, Universidad Nacional de Río Cuarto, Ruta 36, Km 601, 5800 Río Cuarto, Argentina*
[3]*Facultad de Ciencias Químicas, Universidad Nacional de Córdoba, Argentina*

During the last decades, quantum dots within the Coulomb blockade regime of transport have been proposed as essential building blocks for a wide variety of nanomachines. This includes thermoelectric devices, quantum shuttles, quantum pumps, and even quantum motors. However, in this regime, the role of quantum mechanics is commonly limited to provide energy quantization while the working principle of the devices is ultimately the same as their classic counterparts. Here, we study quantum-dot-based nanomachines in the Coulomb blockade regime, but in a configuration that resembles the quantum mechanics' paradigmatic experiment: the double-slit. We show that the coherent superposition of states appearing in this configuration can be used as the basis for different forms of "true" quantum machines. We analyze the efficiency of these machines against different non-equilibrium sources (bias voltage, temperature gradient, and external driving) and the factors that limit it, including decoherence and the role of the different orders appearing in the adiabatic expansion of the charge/heat currents.

I. INTRODUCTION

The high degree of control and the discrete energy spectrum of coupled quantum dots (QDs), sometimes referred to as quantum dot molecules, make them especially suitable for the manipulation of charge and energy fluxes in nanoscale. This is crucial for nanoscopic heat and charge management, the development of new quantum information technologies, and the design of different forms of quantum machines.[1–6] In this regard, experimental and theoretical studies have shown that quantum-dot-based designs may provide remarkable performances in thermoelectric devices that exchange electrical and thermal energies.[7–11] The pumping of charge and heat on quantum-dot-based driven systems have been extensively studied. [10,12–24] In recent years, the reverse process in which heat or charge currents are used to propel a mechanical device has also gained considerable attention.[25–37]

In all the above systems, it is assumed that the typical size of the device is smaller than the characteristic coherence length of electrons. It is clear then that quantum mechanics becomes crucial for the description of these forms of nanodevices, which can be put together under the generic name of quantum machines. Depending on the type of energy conversion involved they are usually referenced as (adiabatic) quantum motors, (adiabatic) quantum pumps (or generators), quantum heat engines, or quantum heat pumps.[6,38] In a quantum motor, a dc electric current is transformed into mechanical work while in a quantum pump, an ac electrical or mechanical driving is turned into a dc electric current. Quantum heat engines and heat pumps are very similar systems but the power source involve temperature gradients instead of bias voltages, and the focus is shifted from charge currents to heat currents.

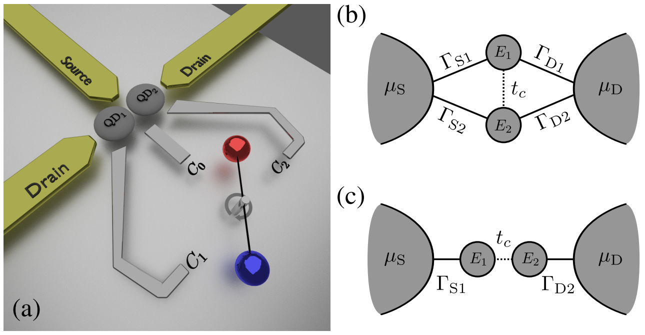

Figure 1. (a) Example of the type of studied systems: a DQD coupled to some mechanical degree of freedom. Here, the dots are weakly coupled to each other and to source/drain leads. The dots' energies are modulated by the gate voltages generated from the capacitive coupling to a charged rotor. Panels (b) and (c) are simplified schemes for the DQD system in parallel and in series, respectively. Lead-dot tunneling events are characterized by four tunneling rates ($\Gamma_{\rm S1}$, $\Gamma_{\rm S2}$, $\Gamma_{\rm D1}$ and $\Gamma_{\rm D2}$) while the interdot coupling is described by t_c. If the two drain leads in (a) are kept at the same voltage, we obtain the parallel configuration. However, by establishing a bias voltage between the two drain leads while removing the source lead in (a), we obtain the series configuration. Throughout this work, the parallel DQD without interdot coupling will be dubbed the double-slit configuration.

The role of quantum mechanics on quantum-dot-based machines strongly depends on the system's conditions. Here, we focus on the *adiabatic* regime, where the modulation of the system's parameters is slow as compared with the typical time spent by the electrons inside it. However, even within this condition there are different transport regimes that should be distinguished. For example, in the ballistic regime, described by a mean-field approximation of the electron repulsion, the working principle of adiabatic quantum pumps and motors can be attributed to interference effects of the electrons passing through the modulation region.[12,26,39–41] On the other hand, in the Coulomb blockade regime, quantum effects are typically restricted to energy quantization so that the internal pumping mechanism, beyond the quantization of the transported charge, resembles that of a classical pump. In this case, some form of rate equation relating the occupation probabilities of the quantum-dot states is typically used to describe the system, while the coherence between them can be disregarded in a first approximation. Quantum pumping,[10,15,22–24,29,42–45] shuttle transport,[37,46] and even adiabatic quantum motors[31] have been studied by using this approach. Other strategies, like the nonequilibrium Green's function formalism, have also been used in the past to study quantum pumping within the Coulomb blockade regime.[47,48] However, the working principle of the device can also be explained by relying on a classical analogous.

Based on the above, it is fair to wonder, once in the adiabatic and Coulomb blockade regimes, how "quantum" a nanomachine based on quantum dots can be. In this context, the weak interdot coupling regime provides a useful platform to test the role of quantum coherences between the dots' states. This is so because the degeneracy of dots' states brings together both occupations and coherences on the same time scale. As a consequence of that, coherences survive even at the steady-state of the system. In particular, in Ref. [49] charge pumping was studied for a double quantum dot (DQD) coupled in series. They found that the coupling between coherences and occupations is responsible for charge pumping. However, given that both coherence and electron transport rely entirely on the interdot coupling, taking the coherence to zero trivially sets the current to zero. Thus, although the "quantumness" of the pumping mechanism is clearly present, its effect is somewhat hidden. On the other hand, in Ref. [50] the authors analyzed charge pumping in an Aharonov-Bohm interferometer configuration of the dots. As in this case there is no explicit interdot coupling, the role of quantum superposition becomes more clear.

In this work, we exploit the weak interdot coupling regime in a DQD to analyze the role of coherence in a broad class of quantum machines such as charge/heat pumps and nanomotors driven by bias voltages or temperature gradients. For this to be achieved, we focus on a particular configuration of the quantum dots, which resembles the double-slit experiment and has no classical counterpart. The configuration consists of a parallel DQD within the Coulomb blockade regime with no direct interdot coupling and where the system is coupled to classical degrees of freedom. The latter provides the dots' energy level modulation. Fig. 1 shows an example of our proposal. Through this model, we show that the above mentioned regime dominated by coherences also applies to quantum motors fueled by a finite bias voltage. In addition, we include in our description an external force acting on the (classical) mechanical component of the system. Such a force allows us to bring together the two operation modes (pump and motor) of the device on a same basis. These ideas are also extended to the case where the leads are subjected to different temperatures, giving rise to coherence induced quantum heat engines and refrigerators. We analyze the performance of these machines and the factors that limit it, including decoherence and the role of the different orders of the adiabatic expansion.

The paper is organized as follows. In Sec. II, we present the theoretical framework, including a brief overview of the real-time diagrammatic approach, the expressions for the observables, the definitions of the efficiencies, and the used decoherence model. In Sec. III, we apply the formalism to the particular example of a DQD weakly coupled to two external leads and capacitively coupled to a rotor. In Sec. IV, we study the performance of the different operational regimes of the double-slit configuration of the DQD. Finally, in Sec. V, we summarize the main results.

II. THEORETICAL FRAMEWORK

A. Hamiltonian model

We consider a system composed of QDs in which mechanical and electronic degrees of freedom are present and coupled to each other. From now on we call this system the *local system*, and we model it by the following Hamiltonian

$$\hat{H}_{\mathrm{local}} = \hat{H}_{\mathrm{el}}(\hat{\boldsymbol{X}}) + \frac{\hat{\boldsymbol{P}}^2}{2m} + U(\hat{\boldsymbol{X}}, t), \tag{1}$$

where $\hat{\boldsymbol{X}} = (\hat{X}_1, ..., \hat{X}_N)$ is the vector (operator) of mechanical coordinates while $\hat{\boldsymbol{P}} = (\hat{P}_1, ..., \hat{P}_N)$ represents their associated momenta, m is the effective mass related to $\hat{\boldsymbol{X}}$, and U denotes some external mechanical potential that may be acting on the local system. We use an explicit time dependence in U to denote that an external and nonconservative force might be acting on the mechanical subsystem (see below). The Hamiltonian $\hat{H}_{\mathrm{el}}$ includes the electronic degrees of freedom of the system, that are participating in the transport, as well as their coupling to the mechanical ones through

$$\hat{H}_{\mathrm{el}}(\hat{\boldsymbol{X}}) = \sum_i E_i(\hat{\boldsymbol{X}})\, |i\rangle\langle i|\,, \tag{2}$$

where the sum runs over all possible electronic many-body eigenstates $|i\rangle$. The system is then weakly coupled to external leads so the *total* Hamiltonian reads

$$\hat{H}_{\mathrm{total}} = \hat{H}_{\mathrm{local}} + \sum_r \hat{H}_r + \hat{H}_{\mathrm{tun}}. \tag{3}$$

The leads are described as non-interacting electrons reservoirs through the Hamiltonian

$$\hat{H}_r = \sum_{k\sigma} \epsilon_{rk} \hat{c}^{\dagger}_{rk\sigma} \hat{c}_{rk\sigma}, \tag{4}$$

where $\hat{c}^{\dagger}_{rk\sigma}$ ($\hat{c}_{rk\sigma}$) is the creation (annihilation) operator for an electron with state-index k and spin projection $\sigma = \{\uparrow, \downarrow\}$ in the lead r, which we typically take as source and drain reservoirs, i.e., $r = \{\mathrm{S}, \mathrm{D}\}$. These reservoirs are assumed to be always in equilibrium, characterized by a temperature T_r and an electrochemical potential μ_r. Finally, the tunnel coupling between the local system and the leads is given by the tunnel Hamiltonian

$$\hat{H}_{\mathrm{tun}} = \sum_{rk\sigma\ell} (t_{r\ell} \hat{d}^{\dagger}_{\ell\sigma} \hat{c}_{rk\sigma} + \mathrm{H.c.}), \tag{5}$$

where $t_{r\ell}$ denotes the tunneling amplitude, which we assume to be k and spin independent for simplicity. The fermionic operator $\hat{d}^{\dagger}_{\ell\sigma}$ ($\hat{d}_{\ell\sigma}$) creates (annihilates) an electron with spin σ in the quantum dot ℓ composing the local system. The tunnel-coupling strengths, defined as $\Gamma_{r\ell} = 2\pi\rho_r |t_{r\ell}|^2$, quantitatively describe the rate at which electrons enter (leave) the quantum dot ℓ from (to) the r-reservoir. We also define the total tunnel rate Γ as $\Gamma = \sum_{r\ell} \Gamma_{r\ell}$. The reservoirs are taken to be in the wideband limit where their densities of states ρ_r are assumed to be energy independent. Throughout this paper, we set $e = 1$ for the absolute value of the electron charge and $\hbar = 1$.

B. Stationary state regime

We suppose that the dynamics of the electronic and mechanical degrees of freedom are well separated from each other, and therefore we can treat them through the Born-Oppenheimer approximation. Under this approximation, the mechanical coordinates can be treated as classical variables obeying the following Langevin-like equation

$$m\ddot{\boldsymbol{X}} + \boldsymbol{F}_{\text{ext}} = \boldsymbol{F} + \boldsymbol{\xi}, \tag{6}$$

where $\boldsymbol{F} = -\langle \nabla \hat{H}_{\text{el}} \rangle = \mathrm{i} \langle [\nabla \hat{H}_{\text{el}}, \hat{\boldsymbol{P}}] \rangle$ is the mean value of the current-induced forces (CIFs) while $\boldsymbol{\xi}$ stands for its fluctuation. Later on we will see that a friction component arises from expanding $\boldsymbol{F}$ in terms of the velocity of the mechanical coordinates.[26,31,51–56] The term $\boldsymbol{F}_{\text{ext}}$ represents an external force applied to the mechanical part of the local system and is related to the potential U in Eq. (1). This force will be, in general, opposed to the bias induced direction of the CIF, so we define it with a minus sign for convenience. As we shall see later, in our model such a quantity appears as the key tool to set up the different operation modes of the electromechanical device. If we manage to calculate the expectation value of the CIF (see Sec. II D) then we can use Eq. (6) to integrate the classical equations of motion and derive the effective dynamics of the local system, including both electronic and mechanical degrees of freedom. In realistic systems, friction and stochastic forces may have different origins, such as the coupling to other phononic degrees of freedom. Here, however, we are only interested in the quantum effects of CIFs. Thus, we will only take into account friction and stochastic forces that arise from the coupling to the electronic degrees of freedom.

Before continuing, some comments about the system are in order. First, we will focus on systems whose mechanical part is capable of reaching a stationary regime characterized by a steady cyclic motion (with some frequency $\Omega \propto \dot{\boldsymbol{X}}$) and whose dynamics can be described by an *angular* Langevin equation. If we assume that this *rotor* follows a circular trajectory then only one parameter, the angle θ, is needed for the study of its dynamics. In this case we can project Eq. (6) on the angular direction $\hat{\boldsymbol{\theta}}$ to obtain the following angular form[6,31]

$$\ddot{\theta} = \frac{1}{\mathcal{I}}(\mathcal{F} - \mathcal{F}_{\text{ext}} + \xi_\theta), \tag{7}$$

where $\mathcal{I}$ is the moment of inertia of the mechanical subsystem, $\mathcal{F}$ is the current-induced torque, $\mathcal{F}_{\text{ext}}$ is the torque associated to the external force, and ξ_θ is the stochastic torque which comes from the angular projection of the CIF's fluctuation.

Second, in addition to the supposition of cyclic mechanical motion, we consider that the terminal velocity reached by the system is constant, i.e. $\dot{\theta} = \Omega$, during the whole cycle. This is also justified for large values of $\mathcal{I}$, where the variation of the angular velocity (together with its fluctuations) along the cycle becomes negligible.[6,27,30,31] Both numerical and analytical procedures for the calculation of $\dot{\theta}$, before and after reaching stationarity, have been carried out in Refs. 31 and 6.

We are now in position to derive a relation between the work related to the torques $\mathcal{F}$ and $\mathcal{F}_{\text{ext}}$. This is done by integrating Eq. (7) over a whole period of the system at the stationary state, yielding[6]

$$\mathcal{W} = \int_0^\tau \mathcal{F}\dot{\theta}\,\mathrm{d}t = \int_0^\tau \mathcal{F}_{\text{ext}}\dot{\theta}\,\mathrm{d}t = \mathcal{W}_{\text{ext}}. \tag{8}$$

The equation implies that, once the cycle is completed, the work related to the CIF is balanced by the work done by the external mechanical force. This equality is fundamental in the sense that it defines the stationary state condition mentioned before and allows us to extract the value of $\dot{\theta} = \Omega$.

C. Generalized master equation

In this section we introduce the formalism that describes the dynamics of the electronic part of the system. This will allow us to calculate the expectation value of the CIF, together with other relevant observables like charge and heat currents, while exactly taking into account the strong Coulomb interaction in the local system. We assume that, before certain initialization time t_0, the leads and the local system are decoupled, such that the total density matrix is factorized as $\hat{\rho} = \hat{p}_{\text{res}} \otimes \hat{p}$. Here $\hat{p}_{\text{res}}$ describes the leads' density matrix, while $\hat{p}$ represents the *reduced* density matrix of the local system. When both subsystems are coupled together, the relevant information of the local system dynamics at times $t > t_0$ is encoded in $\hat{p}(t) = \mathrm{Tr}_{\text{res}}[\hat{\rho}(t)]$, where Tr_{res} is the trace over the reservoirs' degrees of freedom. The time evolution of the matrix elements is governed by the generalized master equation[42]

$$\frac{\mathrm{d}}{\mathrm{d}t} p_\alpha^\beta(t) = -\mathrm{i} \sum_{\beta',\alpha'} L_{\alpha,\alpha'}^{\beta,\beta'}(t) p_{\alpha'}^{\beta'}(t) + \sum_{\alpha',\beta'} \int_{-\infty}^t \mathrm{d}t' W_{\alpha,\alpha'}^{\beta,\beta'}(t,t') p_{\alpha'}^{\beta'}(t'), \tag{9}$$

where $p_\alpha^\beta(t) = \langle \alpha | \hat{p}(t) | \beta \rangle$ and we have taken the limit $t_0 \to -\infty$, in order to neglect any transient effect. The first term in the r.h.s. of this equation takes into account the internal dynamics of the QDs through the Liouvillian superoperator $L\bullet \equiv [\hat{H}_{\rm el},\bullet]$, while the second term describes state transitions due to electron tunneling processes between the leads and the local system. This is quantified by the kernel superoperator W, which represents all irreducible diagrams in the Keldysh double contour,[57] and whose matrix elements $W^{\alpha,\alpha'}_{\beta,\beta'}$ describes the transition between states α' and β' at time t', and states α and β at time t, due to tunnel processes.

To simplify the notation, we gather the diagonal and off-diagonal elements of the reduced density matrix into a vector, $\hat{p} \rightarrow \boldsymbol{p} \equiv (\boldsymbol{p}_{\rm d}, \boldsymbol{p}_{\rm n})^{\rm T}$, yielding a matrix representation for both W and L superoperators, i.e. $W \rightarrow \boldsymbol{W}$ and $L \rightarrow \boldsymbol{L}$. Here, the diagonal and off-diagonal elements of the reduced density matrix are contained in $\boldsymbol{p}_{\rm d}$ and $\boldsymbol{p}_{\rm n}$, respectively. Thus we can think of $\boldsymbol{W}$ and $\boldsymbol{L}$ as composed by the following block matrices

$$\boldsymbol{W} = \begin{pmatrix} \boldsymbol{W}_{\rm dd} & \boldsymbol{W}_{\rm dn} \\ \boldsymbol{W}_{\rm nd} & \boldsymbol{W}_{\rm nn} \end{pmatrix}, \quad \boldsymbol{L} = \begin{pmatrix} \boldsymbol{L}_{\rm dd} & \boldsymbol{L}_{\rm dn} \\ \boldsymbol{L}_{\rm nd} & \boldsymbol{L}_{\rm nn} \end{pmatrix}. \tag{10}$$

As we already mentioned, Eq. (2) tells us that the dots' energy levels are affected by the cyclic mechanical motion, characterized by a frequency Ω proportional to the mechanical velocities $\dot{\boldsymbol{X}}$. If we assume that the dwell time of the electrons in the local system is much shorter than the mechanical period $\tau = 2\pi/\Omega$, then it is possible to perform a frequency expansion on $\boldsymbol{p}(t)$.[6,15,31,42,49] Strictly speaking, this *adiabatic* approximation holds if the adiabaticity condition $\Omega/\Gamma \ll k_{\rm B}T/\delta\epsilon$ is satisfied, where $\delta\epsilon$ stands for the energy amplitude of the QDs' energy levels. This allows us to expand the reduced density matrix as $\boldsymbol{p}(t) = \sum_{k\geq 0} \boldsymbol{p}^{(k)}(t)$ with $\boldsymbol{p}^{(k)} \sim (\Omega/\Gamma)^k$. The first term, $\boldsymbol{p}^{(0)}(t)$, represents the steady-state solution at which the electronic part of the system arrives when the mechanical coordinates are *frozen* at time t. In other words, this order corresponds to the adiabatic electronic response to the mechanical motion. Note that here we are referring to the steady state of the electronic part of the system, which should not be confused with the steady-state regime of the mechanical degrees of freedom mentioned in the previous section. From now on, every time we talk about stationarity, it will be referred to as the mechanical part of the local system. Higher orders terms ($k > 0$) represent nonadiabatic corrections due to retardation effects in the electronic response mentioned earlier.

On top of this adiabatic expansion for small Ω, we perform a perturbative expansion in the tunnel coupling strengths, taking only terms up to first order in Γ (which is reasonable in the weak tunnel coupling limit considered here). Higher-order processes, like cotunneling, are therefore ignored throughout this paper. This double expansion gives rise to the following hierarchy of equations[6,15,31,42,44,49]

$$\begin{aligned} \boldsymbol{W}^{\rm eff}\boldsymbol{p}^{(0)} &= \boldsymbol{0}, \\ \boldsymbol{W}^{\rm eff}\boldsymbol{p}^{(k)} &= \frac{\rm d}{{\rm d}t}\boldsymbol{p}^{(k-1)}, \end{aligned} \tag{11}$$

where we have defined the effective kernel $\boldsymbol{W}^{\rm eff}$ as the zero-frequency Laplace transform of $\boldsymbol{W} - {\rm i}\boldsymbol{L}$, with both matrices evaluated up to first order in Γ. We omit the frequency order superscript in the effective kernel since at this level of approximation it is always $\mathcal{O}(\Omega^0)$. The above set of equations, combined with the normalization condition on the reduced density matrix, $\boldsymbol{e}^{\rm T}\boldsymbol{p}^{(k)} = \delta_{k0}$, allows us to iteratively calculate $\boldsymbol{p}^{(0)}$ and any nonadiabatic correction $\boldsymbol{p}^{(k)}$. The vector $\boldsymbol{e}^{\rm T} \equiv (1,\dots,1,0,\dots,0)^{\rm T}$ is a representation of the local system's trace operator, where the number of ones equals the dimension of the reduced Hilbert space. In light of this, the nonadiabatic corrections can be written as[44]

$$\boldsymbol{p}^{(k)} = \left(\tilde{\boldsymbol{W}}^{-1}\frac{\rm d}{{\rm d}t}\right)^k \boldsymbol{p}^{(0)}. \tag{12}$$

Here $\tilde{\boldsymbol{W}}^{-1}$ represents the pseudo inverse kernel, defined as $\tilde{W}_{ij} \equiv W^{\rm eff}_{ij} - W^{\rm eff}_{ii}$, in order to exclude the zero eigenvalue through the normalization condition. Since the effective kernel is linear in Γ, the k-term of the reduced density matrix, $\boldsymbol{p}^{(k)}$, is proportional to $(\Omega/\Gamma)^k$. This forces us to assume $\Omega < \Gamma$, in order to avoid any divergence.[42] Once we get $\boldsymbol{p}^{(0)}$ and any required nonadiabatic correction $\boldsymbol{p}^{(k)}$, we can proceed with the calculation of all observables related to the performance of adiabatic quantum machines. In the next section we discuss the procedure used to achieve this task.

D. Observables

Now we are going to make use of the formalism described in the previous section to determine the expectation values of a set of observables. First, we consider the charge current $I_r(t) \equiv \langle \hat{I}_r(t)\rangle$ and the heat current $J_r(t) \equiv \langle \hat{J}_r(t)\rangle$, both associated with the r-lead. For these quantities we take the sign convention that in each lead the particle and heat currents are positive when particles and heat are flowing towards the lead, thus we can write the currents in the lead r as

$$I_r(t) = \frac{\rm d}{{\rm d}t}{\rm Tr}[\hat{N}_r\hat{\rho}(t)], \tag{13}$$

$$J_r(t) = \frac{\rm d}{{\rm d}t}{\rm Tr}[(\hat{H}_r - \hat{N}_r\mu_r)\hat{\rho}(t)], \tag{14}$$

where $\hat{N}_r$ is the number operator for the electrons in the reservoir r. We also address the CIF which, unlike the previous observables, constitutes a local quantity. As we showed before, Eq. (2) tells us that the mechanical part of the system only interacts with the local parameters of the dots via their many-body eigenenergies. This implies that the CIF only consists of fermionic dot operators, and therefore we can write its expectation value as

$$\boldsymbol{F}(t) = -\underset{\rm local}{\rm Tr}[\nabla\hat{H}_{\rm el}\hat{p}(t)], \tag{15}$$

where the gradient is taken with respect to the mechanical coordinates $\boldsymbol{X}$.

The adiabatic expansion developed in Sec. II C can also be performed over any observable R of interest (I, J, and F in our case),

$$R(t) = \sum_{k\geq 0} R^{(k)}(t). \tag{16}$$

To lowest order in Γ, the $R^{(k)}$ terms can be written as

$$R^{(k)} = \boldsymbol{e}^{\mathrm{T}} \boldsymbol{W}^{R} \boldsymbol{p}^{(k)}, \tag{17}$$

where $\boldsymbol{W}^{R}$ stands for the kernel associated to the observable R. The charge and heat currents flowing from the lead r into the device are represented by the following kernels[6,10,15,31]

$$[\boldsymbol{W}^{I_r}]_{ij} = -n_i [\boldsymbol{W}^{\mathrm{eff}}_r]_{ij}, \tag{18}$$

$$[\boldsymbol{W}^{J_r}]_{ij} = -(E_i - \mu_r n_i) [\boldsymbol{W}^{\mathrm{eff}}_r]_{ij}, \tag{19}$$

where n_i and E_i are the number of particles and energy associated with the local system's eigenstate $|i\rangle$, respectively, and $\boldsymbol{W}^{\mathrm{eff}}_r$ is the r-lead evolution kernel such that $\boldsymbol{W}^{\mathrm{eff}} = \sum_r \boldsymbol{W}^{\mathrm{eff}}_r$. Regarding the ν component of the CIF, we can directly construct a diagonal matrix kernel from:

$$[\boldsymbol{W}^{F_\nu}]_{ij} = -\frac{\partial E_i}{\partial X_\nu} \delta_{ij}, \tag{20}$$

where again we make use of its local condition.[6,31]

As in the case of $\boldsymbol{p}^{(0)}$, the zeroth-order terms $I_r^{(0)}(t)$ and $J_r^{(0)}(t)$ describe the steady-state currents flowing through the system in a stationary situation where all time-dependent parameters are kept constant at time t. The only way for these terms to be nonzero is when the system is subject to a bias voltage or a temperature gradient since, in this case, the time variation of the mechanical parameters has no effective role in the observables. Higher-order terms represent additional contributions to the steady-state currents due to the delayed response of the system to the mechanical motion.

A similar analysis applies to the CIF, where we take contributions up to first order in the mechanical velocity Ω, i.e. $\boldsymbol{F}(t) = \boldsymbol{F}^{(0)} + \boldsymbol{F}^{(1)}$. The lowest order term can be split into (i) an equilibrium contribution, which is conservative and it can be interpreted as the Helmholtz's free energy of the local system, and (ii) a nonequilibrium term, which appears as a consequence of temperature gradients or bias voltages among the leads.[31] The first adiabatic correction to the CIF, proportional to Ω, gives the frictional force that dissipates energy from the mechanical part of the local system toward the electronic reservoirs.[6] For systems with multiple mechanical degrees of freedom, it also contributes to the energy exchange between modes and, for finite voltages, it can even allow the flux of energy from the leads towards the mechanical degrees of freedom.[51,58]

If we now perform an adiabatic expansion of the torque $\mathcal{F}$, integrate it over a cycle, and use Eq. (8), we get the relation

$$\mathcal{W}_F = s \sum_k \left(\int_0^{2\pi} \frac{\mathrm{d}\theta}{k!} \left. \frac{\partial^k \mathcal{F}}{\partial \dot{\theta}^k} \right|_{\dot{\theta}=0} \right) \dot{\theta}^k = s \sum_k \mathcal{C}_F^{(k)} \dot{\theta}^k, \tag{21}$$

where s is the sign of $\dot{\theta}$ and gives the direction in which the trajectory is traversed. Here, we define the force coefficients $\mathcal{C}_F^{(k)}$ which are independent of the direction of motion of the system, not obvious *a priori*.[6] If we take terms up to $k = 1$, the angular velocity can be obtained from Eq. (21) as follows

$$\dot{\theta} = \Omega = \frac{\mathcal{C}_{\mathrm{ext}} - \mathcal{C}_F^{(0)}}{\mathcal{C}_F^{(1)}}, \tag{22}$$

where we defined $\mathcal{W}_{\mathrm{ext}} = s\mathcal{C}_{\mathrm{ext}}$ to keep track of every term's sign. Note that, for the mechanical subsystem to achieve a stationary regime in the present simple model, the stability condition $\mathcal{C}_F^{(1)} < 0$ should be fulfilled, which implies a positive "friction coefficient".[6]

E. Efficiency

Previously we stated that the mechanical subsystem performs a cyclic motion along a circular trajectory while affecting the dots' energy levels. If we define a closed trajectory $\mathcal{C}$ for the system's parameters that are being modulated, then the work $\mathcal{W}_F^{(0)}$ done by the zeroth-order contribution of the CIF can be calculated by performing a line integral of $\boldsymbol{F}^{(0)}$ along this trajectory or, for two parameters and with the aid of Stokes' theorem, we can calculate it in the following way

$$\mathcal{W}_F^{(0)} = \iint_{\mathcal{S}} \nabla \times \boldsymbol{F}^{(0)} \cdot \mathrm{d}\boldsymbol{S} \equiv \iint_{\mathcal{S}} \boldsymbol{\mathcal{B}}^F \cdot \mathrm{d}\boldsymbol{S}. \tag{23}$$

This means that the work associated with the zeroth-order CIF can be understood as the surface integral of a curvature vector $\boldsymbol{\mathcal{B}}^F = \nabla \times \boldsymbol{F}^{(0)}$ (the curl of the force), which is frequency independent. Analogously, we can define a pumping curvature for the charge current flowing from/to reservoir r as

$$Q_{I_r}^{(1)} = \oint_{\mathcal{C}} \frac{\partial I_r^{(1)}}{\partial \dot{\boldsymbol{X}}} \cdot \mathrm{d}\boldsymbol{X} = \iint_{\mathcal{S}} \boldsymbol{\mathcal{B}}^{I_r} \cdot \mathrm{d}\boldsymbol{S}, \tag{24}$$

and the same can be done for the pumped heat $Q_{J_r}^{(1)}$, via the curvature $\boldsymbol{\mathcal{B}}^{J_r}$. These relations (which are only valid to first order in Ω) highlight the geometrical nature of these observables in the sense that they only depend on the chosen trajectory $\mathcal{C}$.[15,45,59]

Equations like (23), (24), and similar provide a geometrical approach to the study of adiabatic quantum devices, which has been discussed by several authors.[12,59–61] One immediate conclusion from these equations is that the trajectory followed by the modulation parameters should enclose a finite area. This implies that there must be at least two out-of-phase parameters modulating the device.

With the help of the geometric curvatures $\boldsymbol{\mathcal{B}}^F$, $\boldsymbol{\mathcal{B}}^{I_r}$, and $\boldsymbol{\mathcal{B}}^{J_r}$, one can set a convenient working point in the parameters' space around which a trajectory $\mathcal{C}$ will be defined. For example, if the goal is to design a nanomotor, this trajectory should enclose regions of large $\mathcal{B}^F$. On the other hand, if a charge pump is desired, then we should create a closed trajectory over regions where $\mathcal{B}^{I_r}$ is large. All these quantities, together with their integrals, are not independent but related via order-by-order energy conservation, the second law of thermodynamics, and Onsager's reciprocal relations.[4–6,28,38] The order-by-order energy conservation is given by[6,15]

$$\sum_r \left(Q_{I_r}^{(k)} \delta V_r + Q_{J_r}^{(k)} \right) = -\mathcal{W}_F^{(k-1)}. \tag{25}$$

Here, the superscript (k) indicates the order in the frequency expansion and $\delta V_r = \delta\mu_r / e$ where $\delta\mu_r = \mu_r - \mu_0$ (μ_0 is the reference chemical potential). The second law of thermodynamics can be expressed in the following form for the type of systems treated here[6]

$$\sum_k \left[\mathcal{W}_F^{(k)} + \sum_r \left(Q_{I_r}^{(k)} \delta V_r + Q_{J_r}^{(k)} \frac{\delta T_r}{T_r} \right) \right] \leq 0, \qquad (26)$$

where $\delta T_r = T_r - T_0$ (T_0 is the reference temperature). Onsager's reciprocal relations appear in the linear regime of transport, characterized by low bias voltages, small temperature gradients, and low velocities of the moved parameters.[26,38] For example, in a two-lead configuration with $r = \{\mathrm{S}, \mathrm{D}\}$ and when the leads are kept at the same temperature (i.e. $\delta T_r = 0$), Onsager's reciprocal relations imply

$$\tilde{Q}_I^{(1)} \Delta V = -\mathcal{W}_F^{(0)}, \qquad (27)$$

where $\tilde{Q}_I^{(1)} \equiv \tilde{Q}_{I,\mathrm{S}}^{(1)}$, $\Delta V = \delta V_\mathrm{S} - \delta V_\mathrm{D}$, and we use a tilde in the pumped charge to denote that this quantity is being evaluated in the limit of zero bias. Similarly, when no bias voltage is applied between the contacts we have

$$\sum_r \tilde{Q}_{J_r}^{(1)} \frac{\delta T_r}{T_r} = -\mathcal{W}_F^{(0)}, \qquad (28)$$

where, again, the tilde states that the pumped heat is evaluated at zero thermal gradient between the leads.

Eq. (26) allows us to derive bound expressions for the device's efficiencies which, as usual, are defined as the ratio between the output and input powers per cycle.[6] Before doing this, we first need to know how to determine the operational mode of the device, namely, whether the device acts like a motor or a pump. Using Eq. (22), the sign s of the constant velocity $\dot{\theta}$ can be determined and, with it, the sign of $\mathcal{W}_\mathrm{ext}$. The latter determines the direction of the energy flux between the local system and the external agent that is acting on it through U, see Eq. (1). If $\mathcal{W}_\mathrm{ext} > 0$, the energy current flows from the leads to the dots and, there, it is transformed into mechanical work, so the device operates as an electric motor/heat engine depending on the nonequilibrium source. On the contrary, if $\mathcal{W}_\mathrm{ext} < 0$ the external agent is performing mechanical work which is then dissipated through the dots to the leads, so the device operates as a pump.

Now considering that only a bias voltage is applied, the generated electrical current delivers an input energy $Q_I \Delta V$ per cycle, while the output energy is $W_\mathrm{ext} = \mathcal{W}_F^{(0)} + \mathcal{W}_F^{(1)}$. Thus, the efficiency of this *electrical motor* is given by

$$\eta_\mathrm{em} = -\frac{\mathcal{W}_F^{(0)} + \mathcal{W}_F^{(1)}}{\Delta V \left(Q_I^{(0)} + Q_I^{(1)} + Q_I^{(2)} \right)} \leq 1, \qquad (29)$$

in consistence with Eqs. (25) and (26) for a truncation in the frequency expansion up to first order in the CIF, that implies a second-order term in the currents.[6,15] In the opposite case where $\mathcal{W}_\mathrm{ext} < 0$, now the input and output energies swap roles, so the efficiency of this *electrical pump* is

$$\eta_\mathrm{ep} = -\frac{\Delta V \left(Q_I^{(0)} + Q_I^{(1)} + Q_I^{(2)} \right)}{\mathcal{W}_\mathrm{ext}} \leq 1. \qquad (30)$$

Such a quantity, however, is only well defined in the case where the total amount of pumped charge is opposed to that given by the natural direction of the bias current. In the used sign convention for the charge currents this means that $Q_I \Delta V > 0$.

A similar analysis can be done in the case where one replaces the bias voltage by a temperature gradient between the contacts, such that the device can operate either as a heat engine or a refrigerator. By establishing different temperatures in the leads, defined as $T_\mathrm{hot} = T + \Delta T/2$ and $T_\mathrm{cold} = T - \Delta T/2$, a heat current flows through the DQD system which, in turn, may activate its mechanical component. In this scenario where $\mathcal{W}_\mathrm{ext} > 0$, the device is driven by the heat current coming from the hot lead, $-Q_{J_\mathrm{hot}}$. This means that the device operates as a *heat engine* with efficiency:

$$\eta_\mathrm{he} = -\frac{\mathcal{W}_F^{(0)} + \mathcal{W}_F^{(1)}}{Q_{J_\mathrm{hot}}^{(0)} + Q_{J_\mathrm{hot}}^{(1)} + Q_{J_\mathrm{hot}}^{(2)}} \leq \frac{\Delta T}{T_\mathrm{hot}}, \qquad (31)$$

where Q_{J_hot} is defined as the time integral of J_hot over a period given by Ω, while J_hot is taken up to second order in this quantity. On the other hand, when $\mathcal{W}_\mathrm{ext} < 0$ the heat current flows against the temperature gradient. Assuming that the total amount of pumped heat to the cold reservoir is negative, $Q_{J_\mathrm{cold}} < 0$, we can define the efficiency (or coefficient of performance) of this *heat pump* or *refrigerator* by the expression:

$$\eta_\mathrm{hp} = \frac{Q_{J_\mathrm{cold}}^{(0)} + Q_{J_\mathrm{cold}}^{(1)} + Q_{J_\mathrm{cold}}^{(2)}}{\mathcal{W}_\mathrm{ext}} \leq \frac{T_\mathrm{cold}}{\Delta T}, \qquad (32)$$

where again the heat current J_cold is taken up to second order in Ω.[6]

Finally, it is convenient to define normalized efficiencies with respect to the maximum theoretical value, given by Eqs. (31) and (32), i.e.

$$\tilde{\eta}_\mathrm{he} = \frac{T_\mathrm{hot}}{\Delta T} \eta_\mathrm{he}, \quad \text{and} \quad \tilde{\eta}_\mathrm{hp} = \frac{\Delta T}{T_\mathrm{cold}} \eta_\mathrm{hp}. \qquad (33)$$

F. Decoherence model

One of the key questions motivating this work is whether quantum coherence play a role in the operation of QD-based nanodevices such as adiabatic quantum motors and pumps. In this regard, studying the effect of decoherence on the machines' performance is crucial.

Calculating decoherent relaxation times from a microscopic theory would require identifying the dephasing mechanisms, which is beyond the scope of this work. Instead, we choose a phenomenological approach[14,62] that consists of inserting the relaxation times directly into the master equations. In our case, this implies adding to the kernel $\boldsymbol{W}^\mathrm{eff}$ a decoherent rate $\Gamma_\phi \equiv 1/T_2$.[63] The inclusion of Γ_ϕ is only done in the diagonal elements of the nn block of $\boldsymbol{W}^\mathrm{eff}$, i.e. $[\boldsymbol{W}_\mathrm{nn}^\mathrm{eff}]_{ii} \to [\boldsymbol{W}_\mathrm{nn}^\mathrm{eff}]_{ii} - \Gamma_\phi$. The phenomenological rate Γ_ϕ describes any decoherent process that may occur in the quantum dots, present even in the absence of a coupling to the leads. This type of decoherence destroys the information about the relative phase in a superposition of states α and β (p^{α}_{β}) without changing the populations of the states (p^{α}_{α} and p^{β}_{β}). Without a coupling to the reservoirs, this formally leads to a decay of the off-diagonal matrix element $p^{\alpha}_{\beta}(t)$. In our case, however, there is also a replenishing mechanism given by the fact that when electrons enter into the system, they do it in a superposition state. Therefore, it is expected that coherences p^{α}_{β} reach a Γ_{ϕ}-dependent steady-state at long times. In the following sections, we will take Γ_{ϕ} as an "external knob" that can be used to test the effect of decoherence on the machines' performance.

III. DQD IN THE WEAK INTERDOT COUPLING REGIME

In this section we will apply the formalism and assumptions described previously to the particular example of a double dot weakly coupled to two external leads and capacitively coupled to a rotor.

A. Hamiltonian and physical model

The local system we are about to study is a DQD device composed of two single-level spin-degenerate quantum dots coupled to each other, together with a rotative mechanical piece placed in their proximity and capacitively coupled to them. At the same time, the whole device is weakly coupled to source ($r = \mathrm{S}$) and drain ($r = \mathrm{D}$) leads, as depicted in Fig. 1. By weak coupling we mean that the broadening due to tunneling events is much smaller than the temperature broadening, i.e., $\Gamma \ll k_{\mathrm{B}}T$. Notice that, depending on the choice of the tunnel rates $\Gamma_{r\ell}$, it is possible to configure the double quantum dot arrangement either in series or in parallel [see Figs. 1(b) and (c)]. The asymmetry between source and drain rates is quantified by the factor

$$\lambda = (\Gamma_{\mathrm{S}} - \Gamma_{\mathrm{D}})/\Gamma, \tag{34}$$

where $\Gamma_r = \Gamma_{r1} + \Gamma_{r2}$. In addition, for a specific lead $r = \{S, D\}$, we define the lead-dot asymmetry factor as

$$\lambda_r = (\Gamma_{r1} - \Gamma_{r2})/\Gamma_r. \tag{35}$$

These factors will be useful later on for setting different system configurations and for the search of a suitable working point (see Secs. III C and IV). The local system is represented by the electronic Hamiltonian

$$\begin{aligned}\hat{H}_{\mathrm{el}} = &\sum_{\ell} E_{\ell}\hat{n}_{\ell} + U\hat{n}_1\hat{n}_2 + \frac{U'}{2}\sum_{\ell}\hat{n}_{\ell}(\hat{n}_{\ell}-1)\\ &- \frac{t_c}{2}\sum_{\sigma}(\hat{d}^{\dagger}_{1\sigma}\hat{d}_{2\sigma} + \mathrm{H.c.}),\end{aligned} \tag{36}$$

where $\hat{n}_{\ell}$ is the ℓ-dot particle number operator, defined as $\hat{n}_{\ell} = \sum_{\sigma}\hat{d}^{\dagger}_{\ell\sigma}\hat{d}_{\ell\sigma}$, while $E_{\ell} = E_{\ell}(\boldsymbol{X})$ represents the onsite energy of each dot $\ell = \{1, 2\}$, which is locally tuned by its coupling to the mechanical part of the system. t_c denotes the interdot coupling amplitude while U and U' represent the inter and intradot Coulomb interactions, respectively. For the sake of simplicity, we will take in the following these parameters to be much larger than all other energy scales in the system ($U, U' \to \infty$), such that the double-dot device can only be singly occupied or empty. Due to these assumptions, the only states relevant for our system are $|0\rangle$ and $|\ell\sigma\rangle$, where the former means that both quantum dots are empty and the latter that there is one electron with spin σ in the dot ℓ.

Applying a bias voltage and/or a temperature gradient between the leads will cause charge and heat to flow through the dots. If the mechanical piece is coupled to the DQD then an energy exchange between these subsystems is possible. As Fig. 1(a) suggests, the cyclic motion of the rotor (which can be thought of as an electrical dipole) modifies the quantum dots energy levels, similarly to the action of externally controlled gate voltages. In agreement with Eqs. (25)-(28), once a bias voltage or a temperature gradient is applied, the current flowing through the dots release part of its energy to the mechanical subsystem making it to rotate. The opposite scenario can be achieved by applying an external force into the mechanical system, such that its motion produces a finite current through the electronic device. In App. A we discuss in more detail the example shown in Fig. 1(a) and how it might be possible to control the coupling between the quantum dots and the rotor. Another possibility could be a dipolar molecule in proximity to the quantum dots such that there exists a capacitive coupling between the subsystems. In any case, for the purpose of the present work, it does not really matter the specific details of the mechanical system, but its effects on the electronic Hamiltonian. What enables this energy conversion is the dependence of the energy levels of the dots on the position of the mechanical rotor, which in this case can be characterized by an angle θ. This θ-dependence is related to physical characteristics such as the rotor's length and its position with respect to the DQD, and the coupling strength between the rotor and the dots. A strict derivation of this angular dependence requires an accurate knowledge of the rotor's details, which can yield complex parameterizations for the dots' onsite energies. As the aim of the work is to unveil the role of coherences on CIFs and not to focus on specific details of a particular device, we assume a simple θ-dependence for the dots' energies, given by

$$\begin{aligned}E_1(\theta) &= \bar{E}_1 + \delta_E\cos(\theta) + \delta_{\epsilon}\sin(\theta),\\ E_2(\theta) &= \bar{E}_2 + \delta_E\cos(\theta) - \delta_{\epsilon}\sin(\theta),\end{aligned} \tag{37}$$

where δ_E and δ_{ϵ} describe the electromechanical coupling. According to the model shown in Fig. 1(a) and discussed in App. A, they are related to the capacitances acting on the DQD. In the energy space, these equations describe an elliptic trajectory of radius δ_E and δ_{ϵ} around the *working point* $(\bar{E}_1, \bar{E}_2)$. This trajectory is convenient given the typical shape of the curvatures for the configuration of interest of the DQD, see Fig. 3-(a) for example. We assume that these energies $\bar{E}_{\ell}$ can be externally tuned (for example, by external gate voltages) so that the working point can be chosen favorably. If we are thinking in the performance of motors or pumps, then this convenience lies on the fact that, to get useful work or pumped charge/heat, we need to find some region in the parameter space where their associated curvatures are non-zero (cf. Sec. II E). Obviously, the above parametric approach also applies to the energy difference $\epsilon = E_1 - E_2$ and the mean level energy $E = (E_1 + E_2)/2$, such that these can also be treated as tunable parameters through the following equations:

$$E(\theta) = \bar{E} + \delta_E \cos(\theta), \text{ and } \epsilon(\theta) = \bar{\epsilon} + 2\delta_\epsilon \sin(\theta). \quad (38)$$

Importantly, at the level of approximation used in this work, the energy difference between the dots needs to be taken perturbatively, i.e. $\epsilon \sim \Gamma$. As we shall see next, the regions in which the curvature associated with the CIF is non-zero lies below this constrain, such that we can safely define a trajectory enclosing the relevant region of $\mathcal{B}^F$ with δ_ϵ on the order of Γ.

B. Regime of parameters

With the purpose of studying the potential role of quantum coherences on these devices, we will now focus on the weak interdot coupling regime where $t_c \sim \Gamma$. Adiabatic quantum motors, heat engines, and charge/heat pumps, in the strong coupling regime ($t_c \gg \Gamma$) has already been addressed.[6,15,31,49] There, it was shown that coherences have no important contributions to any of the quantities of interest (e.g., charge and heat currents, CIFs, etc.) and can therefore be disregarded to lowest order in Γ. On the contrary, in the weak coupling regime, the role of the coherent superposition among the DQD states becomes crucial for the operation of electron pumps. This was studied in Ref. [49]. Due to the connection between adiabatic quantum motors and pumps [cf. Eq. (25)-(28)], it is expected that coherent effects are also relevant for the performance of quantum motors and heat engines in the weak coupling regime.

Whether or not a system is in the weak or in the strong coupling regimes depends on the comparison between Γ and the energy difference between the eigenstates of the system. When this difference is much bigger than Γ, coherent effects can be disregarded, at least to the lowest order in Γ.[64,65] Here we are in the opposite case, which occurs when both ϵ and t_c are of the order of Γ. The assumption implies that single-electron states are almost-degenerate and guarantees the coherences' survival,[49] laying the ground for the study of their potential effect on autonomous quantum machines like the one studied here.

With respect to the kernel $\boldsymbol{W}^{\text{eff}}$, see Eqs. (10), (11) and App. B, all kernel blocks depend on the mean level energy E. However, the ϵ-dependence only enters in the $\boldsymbol{W}^{\text{eff}}_{\text{nn}}$ block, which contains local information of the system through the Liouvillian $\boldsymbol{L}$. As discussed before in section II E, the geometrical nature of the first-order pumped charge and heat, and the zero-order work of CIFs implies that a two-parameter dependence is necessary for these quantities to be nonzero. In our system, this condition can only be fulfilled if there is a coupling between the diagonal and non-diagonal blocks of $\boldsymbol{W}^{\text{eff}}$. The coupling of the kernels' blocks inevitably leads, in turn, to the coupling of occupations and coherences of the reduced density matrix. Therefore, we can state that occupations and coherences need to be coupled to have finite pumping/work in DQD-based nanodevices within the weak coupling regime.

In the present regime, the single dot states $|\ell\sigma\rangle$ already form the local eigenbasis to compute the density matrix.[49,64] The vector $\boldsymbol{p}$ then adopts the form $\boldsymbol{p} = \left(p_0^0, p_{1\uparrow}^{1\uparrow}, p_{1\downarrow}^{1\downarrow}, p_{2\uparrow}^{2\uparrow}, p_{2\downarrow}^{2\downarrow}, p_{1\uparrow}^{2\uparrow}, p_{1\downarrow}^{2\downarrow}, p_{2\uparrow}^{1\uparrow}, p_{2\downarrow}^{1\downarrow}\right)^{\text{T}}$. Its components represent the occupation probabilities for the device to be either in the empty state $|0\rangle$ (p_0^0) or in the singly occupied state $|\ell\sigma\rangle$ ($p_{\ell\sigma}^{\ell\sigma}$), and coherent superpositions between single particle eigenstates $|\ell\sigma\rangle$ and $|\ell'\sigma\rangle$ ($p_{\ell\sigma}^{\ell'\sigma}$). As we shall see later on, when the DQD is connected in series, such a coupling will be provided by t_c. However, in the parallel configuration we will see that even in the absence of t_c, the coupling between $\boldsymbol{p}_{\text{d}}$ and $\boldsymbol{p}_{\text{n}}$ still holds. This is due to the fact that, under this condition, electrons coming from the leads enter into the DQD in a coherent superposition of states.

C. Role of coherences and the double-slit configuration

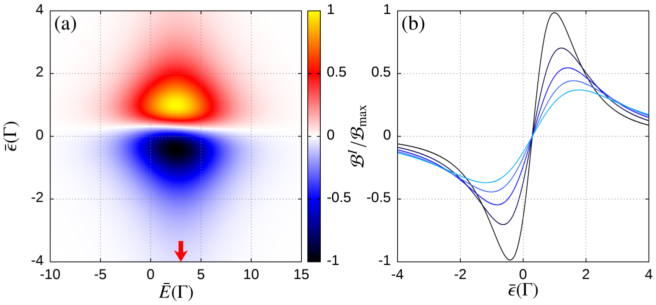

Figure 2. (a) Map of the charge current curvature $\mathcal{B}^I$ as a function of $\bar{E}$ and $\bar{\epsilon}$ for a DQD in series and in the absence of bias voltages and temperature gradients. The shown curvature is normalized to its maximum absolute value within the shown map, $\mathcal{B}_{\max} \sim 0.06\, e/(k_{\text{B}}T)^2$. (b) A cut of the curvature for $\bar{E} = 3\Gamma$ [see red arrow in (a)] and for several decoherence rates: $\Gamma_\phi = 0, 0.25, 0.5, 0.75$, and 1, in units of Γ. The darkest curve corresponds to the case where there is no decoherence ($\Gamma_\phi = 0$) while the lightest one denotes the case of highest decoherence rate ($\Gamma_\phi = \Gamma$). The rest of the curves are for intermediate values of Γ_ϕ. The other parameters used are $\Gamma = t_c = 0.5\, k_{\text{B}}T$, $\lambda = 0.5$, $\lambda_{\text{S}} = 1.0$, and $\lambda_{\text{D}} = -1.0$.

A serially coupled DQD in the weak interdot coupling regime was considered in Ref. [49]. There it was shown that the system is capable of pumping charge without an applied bias voltage if the DQD is asymmetrically coupled to the leads ($\lambda \neq 0$). This can be seen in Fig. 2(a) where we show a map of the charge current curvature $\mathcal{B}^I$ as a function of $\bar{E}$ and $\bar{\epsilon}$. This quantity allows one to determine those regions in the space of parameters over which a closed trajectory can be traced for the production of a net pumped charge current after one modulation cycle.[45] In the figure, we observe a two-lobe pattern with opposite signs. The shift of sign of the current curvature is due to a renormalization of energy levels attributed to the Coulomb interaction.[49,64] As discussed in section II E, moving the parameters E and ϵ such as their trajectory encircles any region of Fig. 2(a), without a change of sign, ensures a finite pumped charge. This alone proves that the system can be used as an adiabatic quantum pump.

The configuration in series of the DQD, see Fig. 1(c), allows one to access different operational modes of the device, i.e., adiabatic quantum motors, adiabatic quantum pumps, etc. However, in this case, quantum coherences come entirely from the coupling between the quantum dots, i.e., the superposition states form when electrons hop sequentially from one dot to the other. This is clear also when one analyses the structure of the effective kernel $\boldsymbol{W}^{\text{eff}}$. There, for the series configuration, the nd and dn blocks of the effective kernel are only given by the local Hamiltonian, such that:

$$\boldsymbol{W}^{\text{eff}}_{\text{dn/nd}} = -\text{i}\boldsymbol{L}_{\text{dn/nd}}. \tag{39}$$

These blocks are responsible for the arising of coherences and for the coupling with the $\boldsymbol{W}^{\text{eff}}_{\text{nn}}$ block (which ultimately leads to finite pumping). In this configuration, all matrix elements in $\boldsymbol{W}^{\text{eff}}_{\text{dn/nd}}$ are proportional to t_c, i.e., there are no contributions from the evolution kernel $\boldsymbol{W}$. Thus, e.g., taking $t_c = 0$ not only destroys any coherent superposition but also trivially cuts charge/heat transport through the local system. In this sense, the parallel configuration of the DQD, see Fig. 1(b), offers a richer example to study the role of coherences. There, coherences do not solely come from the interdot coupling but also from the particles entering simultaneously to both dots. This comes from the fact that novel tunnel processes are enabled, since the matrix elements of $\boldsymbol{W}_{\text{nd/dn}} \propto t_{r,1}t^*_{r,2}$ become non-zero (see App. B).

In contrast to the configuration in series, in the parallel scenario it is possible to pump charge or heat even if the dots are decoupled ($t_c = 0$), see Fig. 3(a). This particular case does not have a classical analogous as classical particles entering one dot, do not have a way of getting information from the other one. Then, a “classical” DQD should behave as two independent single parameter systems and, because of that, the total pumped charge, e.g., should be zero. Therefore, the quantum nature of electrons, which allows for a coherent superposition of the wave functions, it is the ultimate responsible for the pumping of charge and heat, and the production of finite work from the CIFs. One can interpret that quantum coherences are what allows a particle to get information from both dots making the pumping to depend on two parameters, E_1 and E_2 (or E and ϵ). In this sense, devices based on this configuration can be considered as “true” quantum machines. Because of the similarity between the DQD in parallel with $t_c = 0$ and the paradigmatic double-slit experiment we dubbed this the “double-slit” configuration of the DQD.

Before analyzing the effect of decoherence on the series and double-slit configuration of the DQDs, we want to analyze an interesting case of the system’s parameters that leads to zero pumping. As we pointed out before, the coupling between the E-dependent block of the effective kernel ($\boldsymbol{W}^{\text{eff}}_{\text{dd}}$) and the ϵ-dependent one ($\boldsymbol{W}^{\text{eff}}_{\text{nn}}$), is what provides the two parameters needed for finite pumping. However, even in the presence of such a coupling, we found that setting $\lambda_{\text{S}} = \lambda_{\text{D}}$ leads to zero pumping, in the absence of a bias voltage or a temperature gradient, independently of the choice of λ. This occurs despite the fact that there is no obvious inversion symmetry [see Eqs. (34) and (35)] and even when parameters E and ϵ enclose a finite area in the parameters’ space. However, this particular case can be understood once one realizes that the pumping currents become proportional to each other: $I^{(1)}_r = (\Gamma_r/\Gamma_{r'})I^{(1)}_{r'}$, where $r, r' = \{\text{S}, \text{D}\}$, see App. C. The proportionality between both currents implies that each one can be written as the total time derivative of the average zeroth-order occupation number $\langle\hat{n}\rangle$ and, thus, they integrate to zero for a whole cycle, see App. C.

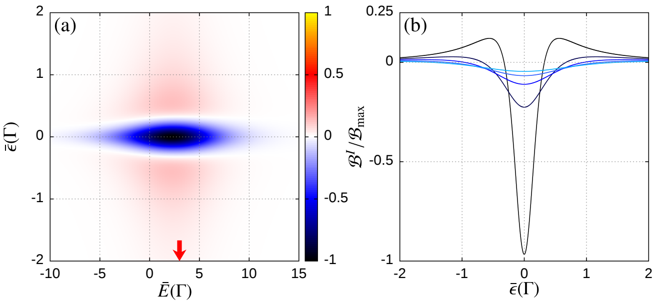

Figure 3. (a) Map of the charge current curvature $\mathcal{B}^I$ as a function of $\bar{E}$ and $\bar{\epsilon}$ for a DQD in parallel and in the absence of bias voltages and temperature gradients. The shown curvature is normalized to its maximum absolute value $\mathcal{B}_{\text{max}} \sim 0.5\,e/(k_{\text{B}}T)^2$ whithin the shown map. (b) A cut of the pseudomagnetic field for $\bar{E} = 3\Gamma$ [see red arrow in (a)] and for several decoherence rates: $\Gamma_\phi = 0, 0.25, 0.5, 0.75$, and 1, in units of Γ. The darkest curve corresponds to the case where there is no decoherence ($\Gamma_\phi = 0$) while the lightest one denotes the case of highest decoherence rate ($\Gamma_\phi = \Gamma$). The rest of the curves are for intermediate values of Γ_ϕ. The used parameters are $\Gamma = 0.5\,k_{\text{B}}T$, $t_c = 0$, $\lambda = 0$, $\lambda_{\text{S}} = 0.5$, $\lambda_{\text{D}} = -0.5$.

As a way to test the role coherences on DQD-based quantum machines in the series configuration, we show in Fig. 2(b) the current curvature for a fixed mean energy, $\bar{E} = 3\Gamma$, and different decoherence rates Γ_ϕ. There it can be seen that Γ_ϕ produces an amplitude decay and a widening of the curvature peaks which can be attributed to a gradual attenuation in the coherent coupling between the quantum dots. Interestingly, for intermediate values of Γ_ϕ there are some regions in parameter’s space where decoherence increases the magnitude of the curvature due to its broadening effect, see for example $\bar{\epsilon} \sim 3\Gamma$.

In Fig. 3(a) we show the current curvature $\mathcal{B}^I$ but for the double-slit configuration. Now, we observe a three-lobe pattern but dominated by a single sign (here the absolute value of the central peak is much greater than that corresponding to the side peaks). The role of Γ_ϕ on the curvature, see Fig. 3(b), is the same as in the configuration in series, but the fact that $t_c = 0$ in this case, allows us to give a more direct interpretation of its effect for sufficiently large values. In this limiting situation, the two dots become effectively decoupled since the characteristic survival time of the superposition now goes like $1/\Gamma_\phi$. Then, each dot is unaware of the other dot’s existence as all phase information gets lost much faster than the typical time spent by the electron in the DQD system. As mentioned, this leads to a monoparametric scheme (with E the only parameter being modulated), such that $\mathcal{B}^I \to 0$ and therefore no working device can be created.

IV. QUANTUM MACHINES BASED ON THE DOUBLE-SLIT DQD

In the previous section, we discussed the role of coherence in charge pumping, but the studied device admits other operational regimes. Here, we study the effects of applying an external driving force together with a bias voltage or a temperature gradient to the double-slit configuration. This takes the system into different operational regimes, namely: electric motor, charge pump, heat engine, or heat pump. We start by describing the effect of a bias voltage and an external force.

The shown charge current curvatures in Figs. 2 and 3 are clear indications that the device may operate as a charge pump in the situation where there is no applied bias voltage. Although not shown, the force curvature $\mathcal{B}^F$ displays a similar pattern thus implying that the device could also work as an electrical motor for the chosen parameters. However, to understand in more detail the device's operational behavior, we need to take into account the effect of the external force $\boldsymbol{F}_{\text{ext}}$. This force will finally determine if the system is operational or not, together with its subsequent working mode, i.e., motor or pump. For simplicity we assume that the external force is constant and points along the tangential direction $\hat{\boldsymbol{\theta}}$, i.e. $\boldsymbol{F}_{\text{ext}} = F_{\text{ext}}\hat{\boldsymbol{\theta}}$, so its associated torque $\mathcal{F}_{\text{ext}}$ is constant along the whole trajectory and we can take $\mathcal{W}_{\text{ext}} = 2\pi s \mathcal{F}_{\text{ext}}$.

One of the interesting aspects of the system analyzed here is that one can control its operational mode externally, shifting from a pump to a motor by moving the bias voltage or the externally applied torque. For the case of the motor, the system will act as such when the work done by the CIFs overcomes the work done by the external agent, $\mathcal{W}_{\text{ext}}$. Then, for a fixed voltage, obviously $\mathcal{F}_{\text{ext}}$ acts as the external knob that controls whether the system is a motor or not. For the case of the charge pump, the system will act as such when the pumped current overcomes the leakage current given by the zero-order contribution (proportional to ΔV at least for small voltages) and the second-order contribution (proportional to Ω^2). For a fixed voltage, here also $\mathcal{F}_{\text{ext}}$ acts as the external knob, but for a different reason. In this case, $\mathcal{F}_{\text{ext}}$ is controlling the compensation between the leakage and pump currents. Note that each order of the current depends differently on Ω which is ultimately controlled by $\mathcal{F}_{\text{ext}}$. One can also take the voltage as the pump knob. Here, one is mainly controlling the zero-order current, which at some point will be so large that it cannot be counteracted by the pumped current. All these features are reflected in the cross-shaped efficiency shown in Fig. 4(a).

In Fig. 4(a) we show a map of the electric motor/pump efficiencies η_{em} and η_{ep} as a function of the external torque $\mathcal{F}_{\text{ext}}$ and the bias voltage ΔV for the double-slit configuration. The plot allows us to visualize the regions in which the device becomes operational, while giving us a quantitative idea on the performance it can reach. The vertical arm of this cross-shaped map corresponds to the motor efficiency [see also panel (b), η_{em} for $\Delta V = 0.3\, k_{\text{B}}T$], while the horizontal arm depicts the charge pump efficiency [see also panel (c), η_{ep} for $\Delta V = 0.03\, k_{\text{B}}T$]. Notice that, in principle, not all regions in the shown map are well defined as the obtained frequencies not always fulfill the adiabaticity condition discussed in Sec. II C and upon which our expansion is justified. Concretely, the unshaded regions in the figures correspond to $\Omega\delta\epsilon/\Gamma k_{\text{B}}T \leq 0.05$, in which our expansion should be adequate.

To evaluate the role of the decoherence in the efficiencies, in Fig. 4(b) and (c) we show η_{em} and η_{ep}, respectively, for a fixed bias voltage and different values of Γ_ϕ. In general, we could say that the decoherence rate has an adverse effect over the device's performance in the sense that it reduces the device's maximum efficiency. This result was expected since, as seen before in Sec. III C, Γ_ϕ tends to reduce the peaks in the curvature $\mathcal{B}^I$ ($\mathcal{B}^F$), which is proportional to the pumped charge (CIF work). For the electric motor this is quite evident as all curves progressively fall off below the zero-decoherence case. Note also that the range within which the device acts as a motor always decreases with Γ_ϕ. This range is determined by the crossing of the curves with the line $\eta = 0$, see Fig. 4(b). For the electric pump, however, the situation is different. There, even though there is an overall decrease of the efficiency, decoherence injection makes the system more resilient to the effects of the external force. In Fig. 4(c) we can see that for $\Gamma_\phi = 0$, the device can only bear torques up to approximately 0.3 $k_{\text{B}}T/\text{rad}$, a small value compared to the torques it can withstand for $\Gamma_\phi > 0$. Interestingly, this allows the system to be "activated" by decoherence in regions where, in principle, it wouldn't be operational. Such effect has already been discussed in a similar quantum system in Ref. [27], where the performance of an adiabatic quantum motor was improved with the aid of decoherence. Notice that, in that case, the electromechanical device was described within the Landauer-Büttiker formalism, as is usual in systems where the Coulomb interaction between electrons can be taken as a mean field. Here we see that a similar decoherence-induced activation appears in the pumping regime under strong Coulomb interaction.

In the energy range shown in Fig. 4(a) and for the considered set of parameters, the maximum efficiency achieved was $\eta_{\max} \approx 0.01$, a small value if one compares it with the strong interdot coupling regime discussed in Ref. [31], where efficiencies up to 75% were obtained. While in the motor operation mode this value can be increased (see below), for the electric pump, the small value of η seems not so easy to overcome. The reason behind that lies in the interplay between the different orders of the transported charge per cycle, $Q_I^{(k)}$, as depicted in Fig. 5(a). Notice that each order obeys a different law as one moves the external torque. This is so because, first, Ω depends linearly on $\mathcal{F}_{\text{ext}}$ [see Eq. (22)], and second, each contribution to the charge current has a different dependence on the angular frequency Ω, i.e., $Q_I^{(k)} \propto \Omega^{k-1}$. Therefore, e.g., in regions where the frequency is extremely small (as compared with Γ), the amount of transported charge in a period is dominated by its zeroth-order contribution, as many

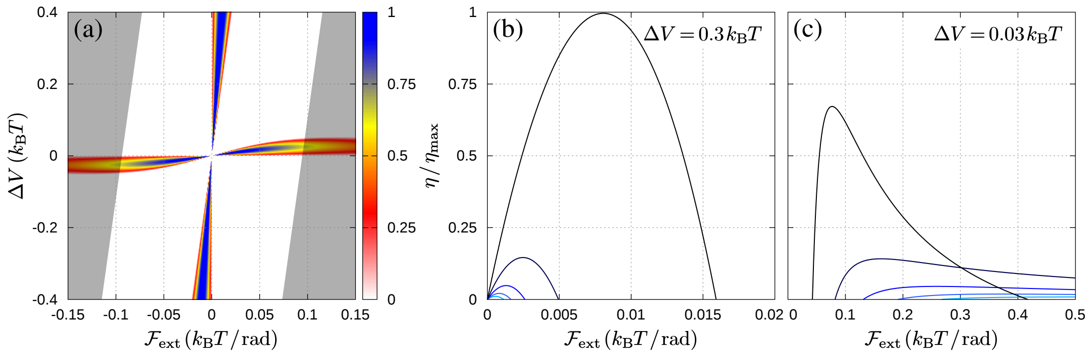

Figure 4. (a) Map of the efficiencies $\eta_{\rm em}$ and $\eta_{\rm ep}$ as functions of the external torque $\mathcal{F}_{\rm ext}$ and the bias voltage ΔV. The efficiencies have been normalized with respect to the maximun value $\eta_{\max} = 1.05 \times 10^{-2}$ achieved in the shown region. Shaded areas denote the regions where the adiabaticity condition is not fulfilled (see main text). (b) Electric motor efficiencies as a function of $\mathcal{F}_{\rm ext}$ for $\Delta V = 0.3\,k_{\rm B}T$ and different decoherence rates in units of Γ: $\Gamma_\phi = 0$ (black), 0.25, 0.5, 0.75, and 1 (cyan). (c) Electric pump efficiencies as a function of $\mathcal{F}_{\rm ext}$ for $\Delta V = 0.03\,k_{\rm B}T$ and the same values of Γ_ϕ as in (b). The other used parameters are $\Gamma = 0.5\,k_{\rm B}T$, $t_c = 0$, $\lambda = 0$, $\lambda_{\rm S} = 0.5$, and $\lambda_{\rm D} = -0.5$. The chosen trajectory is given by $\bar{E} = 1.1\,k_{\rm B}T$, $\bar{\epsilon} = 0$, $\delta_E = 5\,k_{\rm B}T$, and $\delta_\epsilon = 0.15\,k_{\rm B}T$.

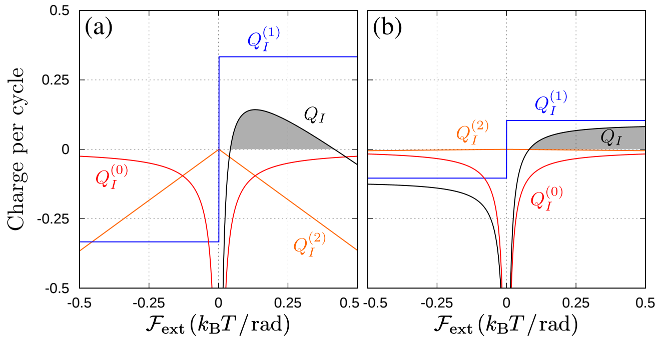

Figure 5. Different order contributions to the transported charge as a function of the external torque $\mathcal{F}_{\rm ext}$. The sum of all these contributions, denoted by Q_I, is shown in solid black. The gray area indicates the region where the device is capable of pumping charge and therefore becomes operational. We considered the same parameters as in Fig. 4(c) with $\Gamma_\phi = 0$ (a) and $\Gamma_\phi = 0.25\Gamma$ (b).

electrons can flow through the system even though the mechanical motion is almost frozen. The first-order contribution, which is the relevant quantity for the device's performance, only surpasses the sum of the other contributions in a small range of the external force, see the gray area in Fig. 5(a). In other words, the first-order current only prevails over the leaking effect, given by the zeroth- and second-order currents, in a small range of $\mathcal{F}_{\rm ext}$. The effect of decoherence on the current is complex, as it affects each order in a different way. Figs. 5 (a) and (b) show an example of this. There, one can notice that, although all contributions to Q_I decrease with an increase of decoherence, the second-order term is affected much dramatically, making it negligible within the shown range of parameters. As a consequence of that, the range over which charge pumping is possible is considerably extended.

As can be seen in Fig. 4(a), increasing ΔV shrinks the region over which charge can be pumped, to the point where this is no longer possible, i.e., $Q_I^{(1)}$ cannot exceed the other contributions. This is expected since dots' energies are very similar in the considered approximation, and hence most of the particles easily flow through the system (along the bias direction) without exchanging its momentum with the mechanical part. Being limited to work only in the low-bias voltage regions makes it difficult to increase efficiency. The situation is quite different for the motor regime. There, the working region is limited by $\mathcal{F}_{\rm ext}$, but CIFs can easily be risen to compensate for that by just increasing ΔV. Therefore, there is more freedom to look through the space of parameters. We perform a wide numerical exploration and find that adiabatic quantum motors can achieve efficiencies up to 50%, but in a large bias regime ($\Delta V \sim 20\,k_{\rm B}T$).

We have also studied other operation regimes of our system. In particular, we explored its role as a heat pump (refrigerator) and as a heat engine (temperature-driven motor), see Fig. 6. The results are similar to those described above for the charge pump and the electric motor regimes. The main differences are: (i) the heat pump is more sensitive to decoherence, see Fig. 6(c) and notice the different Γ_ϕ used values with respect to Fig. 4(c), and (ii) due to the way in which the efficiencies are affected by Γ_ϕ, we can conclude that there is no activation by decoherence at least in this regime of the parameters. We observe that efficiencies of the order of 4% were obtained when taking temperature gradients close to the limit of zero temperature in the cold reservoir [where Carnot's efficiency is 1 and which is out of the range of Fig. 6(a)]. On the other hand, the quantum refrigerator achieves an efficiency which is approximately 2% of Carnot's limit. Again, these values are small when compared to the ones reported for the strong interdot coupling regime, where efficiencies higher than 50% of Carnot's limit were obtained for both the heat engine and the refrigerator operational modes.[6,15] As discussed above, the reason behind these low values lies in the fact that leakage currents are dominant in the considered regime of parameters. In Fig. 7 we show the contributions for the transported heat per cycle as a function of the external torque for $\Gamma_\phi = 0$ and 0.05 Γ. We can see that both the zeroth and second-order trans-

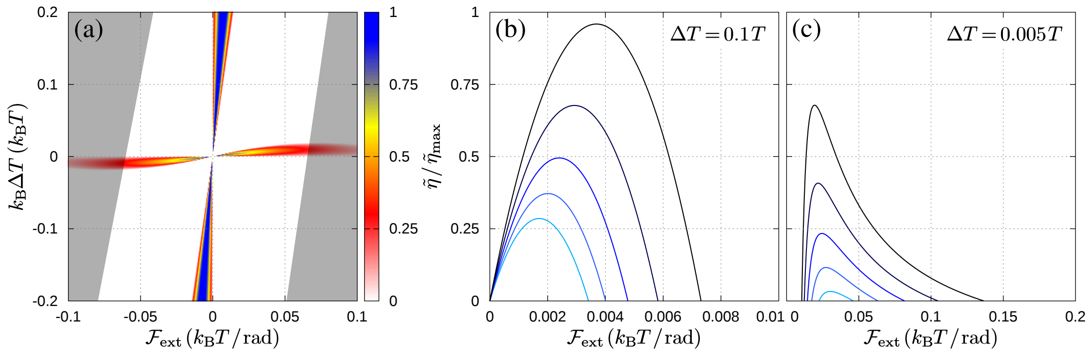

Figure 6. (a) Map of the *normalized* efficiencies $\tilde{\eta}_{\rm he}$ and $\tilde{\eta}_{\rm hp}$ as a function of $\mathcal{F}_{\rm ext}$ and ΔT. These functions have been divided with respect to the maximum value $\tilde{\eta}_{\rm max}=1.04\times10^{-2}$ achieved in the shown map. As in Fig. 4, the shaded areas denote the regions where the adiabaticity condition is not satisfied. (b) Plots of $\tilde{\eta}_{\rm he}$ vs $\mathcal{F}_{\rm ext}$ for $\Delta T=0.1\,T$ and for different decoherence rates (in units of Γ): $\Gamma_\phi=0$ (black), 0.05, 0.1, 0.15, and 0.2 (cyan). (c) Plots of $\tilde{\eta}_{\rm hp}$ vs $\mathcal{F}_{\rm ext}$ for $\Delta T=0.005\,T$ and for the same values of Γ_ϕ as in (b). The other used parameters are: $\Gamma=0.5\,k_{\rm B}T$, $t_c=0$, $\lambda=0$, $\lambda_{\rm S}=0.5$, and $\lambda_{\rm D}=-0.5$. The chosen trajectory is given by $\bar{E}=5\,k_{\rm B}T$, $\bar{\epsilon}=0$, $\delta_E=5\,k_{\rm B}T$, and $\delta_\epsilon=0.2\,k_{\rm B}T$.

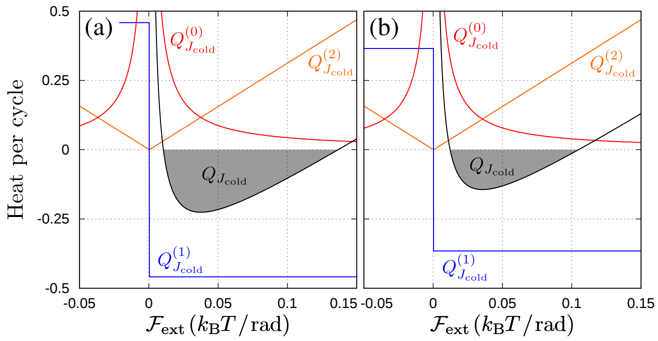

Figure 7. Different order contributions to the transported head from the cold reservoir as a function of the external torque $\mathcal{F}_{\rm ext}$. The sum of all these contributions, denoted by $Q_{J_{\rm cold}}$, is shown in solid black. The gray area indicates the region where the device is capable of pumping heat and therefore becomes operational. We considered the same parameters as in Fig. 6(c) with $\Gamma_\phi=0$ (a) and $\Gamma_\phi=0.05\Gamma$ (b).

ported heat (i.e., those coming from the leakage currents) are almost not affected by decoherence, while the first order contribution clearly decays with Γ_ϕ. Despite that, we remark that the goal of the present work is not to obtain efficient pumps or motors but to study up to what extent coherences may play a role in QD-based quantum machines within the Coulomb blockade regime.

V. CONCLUSIONS

We studied quantum-dot-based nanomachines in the Coulomb blockade regime in a situation where the coherences can dominate the transport properties of the device. We focused our analysis to what we called the double-slit configuration. In this setup, coherences do not come from the interdot coupling, which is zero, but from the particles entering/leaving the two dots simultaneously. Therefore, the only way particles entering the system get information from the two dots is through a coherent superposition of states. This makes the modulation manifold effectively bi-parametric, as required in the adiabatic regime. In this sense, the double-slit configuration can be used as the basis for different forms of "true" quantum machines, namely: quantum motors, quantum pumps, quantum heat engines, and quantum heat pumps.

We analyzed the impact of decoherence on the above machines. As expected, we found that the overall result is to decrease the efficiency of the machines. In the strong decoherence limit, this can be interpreted as the situation in which the quantum superposition is destroyed, so the electrons in the device can no longer access the two parameters, and the amount of pumped charge/heat or useful work per cycle goes to zero. However, for intermediate values of Γ_ϕ, its effect is more complex due to two main factors. The first one is that, although decoherence tends to decrease the maximum of the geometric curvatures (current, heat, and force), it also widens them. This causes that, under specific parameters, some forms of quantum machines can indeed be activated by decoherence, in the sense that they require a minimum amount of it to operate. The other important factor is that decoherence can affect the orders of the adiabatic expansions of the observables differently. This is the reason for the found differences between charge and heat pumps regarding the effect of decoherence on them.

VI. ACKNOWLEDGEMENTS

We acknowledge financial support by Consejo Nacional de Investigaciones Científicas y Técnicas (CONICET); Secretaría de Ciencia y Tecnología de la Universidad Nacional de Córdoba (SECYT-UNC); and Agencia Nacional de Promoción Científica y Tecnológica (ANPCyT, PICT-2018-03587).

Appendix A: Trajectory in the parameter space

In Sec. III A we stated that it is convenient to take an elliptic trajectory around the origin of the energy space in order to take advantage of the shape of $\mathcal{B}^I$ and thus increase the efficiency of the device. More specifically, this elliptic trajectory should be much wider along the E axis than in the ϵ axis [cf. Fig. 3(a)]. With this in mind, we now show how the experimental setup displayed in Fig. 1 can be configured to allow for such a trajectory. Let C_1 and C_2 be the capacitances of the side contacts and C_0 the capacitance of the central contact, displayed in the middle of the two dots. For the considered configuration, the dots' energies can be described by

$$E_i(\theta) = E_i^{(0)} + \frac{q_0(\theta)}{C_0} + \frac{q_i(\theta)}{C_i}, \quad i = \{1,2\}, \tag{A1}$$

where $E_i^{(0)}$ is the energy in the absence of contacts, the q's denote the amount of charge accumulated in each one of the contacts, as a function of the rotor's position. For the specific geometry of the rotor and the used configuration for the contacts, we could argue that $q_1(\theta) = -q_2(\theta)$, as the charges in the rotor are assumed to be the same in magnitude, but opposite in sign. Besides, we could simplify the above dependence by stating that $C_1 = C_2$. Due to the position of the central contact with respect to the C_1 contact, it is reasonable to expect a phase shift of $\pi/2$ in q_0, i.e., $q_1(\theta) = q_0(\theta + \pi/2)$. Accordingly, we replace these assumptions in the above expressions and obtain

$$E_{1,2}(\theta) = E_{1,2}^{(0)} + \frac{q_0(\theta)}{C_0} \pm \frac{q_0(\theta + \pi/2)}{C_1}. \tag{A2}$$

If we now define $E = (E_1 + E_2)/2$, $\epsilon = E_1 - E_2$, $E^{(0)} = (E_1^{(0)} + E_2^{(0)})/2$, $\epsilon^{(0)} = E_1^{(0)} - E_2^{(0)}$, $C_E = C_0$ and $C_\epsilon = C_1/2$, we arrive at the following parametric equations:

$$E(\theta) = E^{(0)} + \frac{q_0(\theta)}{C_E}, \quad \epsilon(\theta) = \epsilon^{(0)} + \frac{q_0(\theta + \pi/2)}{C_\epsilon}. \tag{A3}$$

Thus, if an elliptic trajectory with $E_{\mathrm{max}} \gg \epsilon_{\mathrm{max}}$ is desired, then it is enough to take $C_\epsilon \gg C_E$.

Appendix B: Effective evolution kernel

In this appendix we show how the blocks of the effective evolution kernel $\boldsymbol{W}^{\mathrm{eff}}$ are related to the energy parameters E and ϵ. As discussed in Sec. II C, this effective kernel is defined as the sum of the evolution kernel $\boldsymbol{W}$ and the Liouvillian $\boldsymbol{L}$, which can be decomposed into two contributions, $\boldsymbol{L}_{\mathrm{dot}}$ and $\boldsymbol{L}_c$, by separating the t_c-dependent term in the electronic Hamiltonian of Eq. (36). To study the energy dependence, we will treat these components individually. For the system treated in this work, the matrix elements of the evolution kernel $\boldsymbol{W}$ depend on the DQD's eigenenergies in the following way

$$W_{\beta,\beta'}^{\alpha,\alpha'} \propto \Gamma \sum_{p\eta r} \sum_{ij} \left[-p\phi_r(q_{ij}^{\eta,r}) - \mathrm{i}\pi f(p q_{ij}^{\eta,r}) \right]. \tag{B1}$$

Here, $p = \pm$ is an index that distinguishes forward $(+)$ from backward $(-)$ time evolutions on a Keldysh double contour diagram while $\eta = \pm$ is a particle index denoting the annihilation/creation of an electron in the r-lead. The indexes i and j run over the DQD's eigenstates, and $f(x) = [1 + \exp(x)]^{-1}$ is the usual Fermi function. The function $\phi(x)$ is defined as:

$$\phi_r(x) = -\mathrm{Re}\,\psi\left(\frac{1}{2} + \mathrm{i}\frac{x}{2\pi}\right) + \ln\frac{D}{2\pi k_{\mathrm{B}} T_r}, \tag{B2}$$

where ψ is the digamma function and D denotes the reservoir's bandwidth, which we assume to be independent of r for simplicity. The argument in the above functions corresponds to the energy difference between initial and final eigenstates, with respect to the r-lead electrochemical potential and divided by the thermal energy, i.e.

$$q_{ij}^{\eta,r} = \frac{E_i - E_j - \eta\mu_r}{k_{\mathrm{B}} T_r}. \tag{B3}$$

If we set the energy of the empty state as reference, i.e., $E_0 = 0$, then all non-vanishing elements of $\boldsymbol{W}$ depend only on the energies $E_{\ell\sigma}$ of the singly occupied states. At the same time, as in the approximation mentioned in Sec. III B the effective kernel $\boldsymbol{W}^{\mathrm{eff}}$ must be taken up to first order in Γ, and since all elements in $\boldsymbol{W}$ are multiplied by a prefactor proportional to Γ, the energy differences entering in $q_{ij}^{\eta,r}$ need to be taken up to zeroth order in the perturbation parameter. This means that the arguments $q_{ij}^{\eta,r}$ can only retain the zeroth order contribution, so all elements in $\boldsymbol{W}$ only depend on the mean level energy E.[49,64] If we now consider the Liouvillian $\boldsymbol{L}_c$, we can see that

$$[\boldsymbol{L}_c]_{\beta,\beta'}^{\alpha,\alpha'} = \langle\beta|\,\hat{H}_c\,|\alpha\rangle\,\delta_{\alpha'\beta'} - \langle\alpha'|\,\hat{H}_c\,|\beta'\rangle\,\delta_{\alpha\beta}, \tag{B4}$$

where $\hat{H}_c$ accounts for the interdot coupling Hamiltonian [last term in the r.h.s. of Eq. (36)]. Due to the Kronecker deltas and the off-diagonal structure of $\hat{H}_c$ in the local basis, this Liouvillian will only contribute to the dn and nd blocks of $\boldsymbol{W}^{\mathrm{eff}}$ with terms of the form $\pm\mathrm{i}\,t_c/2$. Lastly, we study the energy dependence of the Liouvillian $\boldsymbol{L}_{\mathrm{dot}}$. In this case it can be shown that

$$[\boldsymbol{L}_{\mathrm{dot}}]_{\beta,\beta'}^{\alpha,\alpha'} = (E_\alpha - E_{\alpha'})\delta_{\alpha\beta}\delta_{\alpha'\beta'}. \tag{B5}$$

This means that $\boldsymbol{L}_{\mathrm{dot}}$ will only contribute to the nn block of $\boldsymbol{W}^{\mathrm{eff}}$. Since we are working in the local basis, this implies that $\boldsymbol{L}_{\mathrm{dot}}$ is diagonal, whose elements are $\pm\epsilon$. The explicit matrix representation of the complete Liouvillian $\boldsymbol{L} = \boldsymbol{L}_{\mathrm{dot}} + \boldsymbol{L}_c$ is thus given by $\boldsymbol{L}_{\mathrm{dd}} = \boldsymbol{0}$,

$$\boldsymbol{L}_{\mathrm{dn}} = \frac{t_c}{2}\begin{pmatrix} 0 & 0 & 0 & 0 \\ 1 & 0 & -1 & 0 \\ 0 & 1 & 0 & -1 \\ -1 & 0 & 1 & 0 \\ 0 & -1 & 0 & 1 \end{pmatrix}, \tag{B6}$$

together with $\boldsymbol{L}_{\mathrm{nd}} = \boldsymbol{L}_{\mathrm{dn}}^{\mathrm{T}}$ and $\boldsymbol{L}_{\mathrm{nn}} = \epsilon\,\mathrm{diag}(1, 1, -1, -1)$. Regarding the decoherence rates, all the blocks of the decoherence matrix $\boldsymbol{\Gamma}_\phi$ are zero, except for the nn block, which is simply Γ_ϕ times the 4×4 identity matrix.

To summarize this analysis, we conclude that all blocks of $\boldsymbol{W}^{\mathrm{eff}}$ are E-dependent but only its nn block depends on the energy difference ϵ. With regard to the interdot coupling, we can see that for the configuration in series, the elements in $\boldsymbol{L}_c$ are the only ones connecting the dd and nn blocks of the effective kernel, such that coherences are completely determined by this parameter. However, in the configuration in parallel, additional matrix elements proportional to $t_{r,1}t^*_{r,2}$ [cf. Eq. (5)] contribute in the dn and nd blocks of $\boldsymbol{W}$, such that coherences may even survive without any interdot coupling.

Appendix C: Symmetric couplings to the leads

Here we go into detail about the recovery of the $\epsilon_1 \leftrightarrow \epsilon_2$ symmetry by taking the same asymmetry factors when coupling the DQD system with the leads, i.e., $\lambda_{\mathrm{S}} = \lambda_{\mathrm{D}}$. Under this condition, the tunneling rates satisfy

$$\Gamma_{r,i} = \frac{\Gamma_r}{\Gamma_{r'}}\Gamma_{r',i}, \tag{C1}$$

where $r, r' = \{\mathrm{S}, \mathrm{D}\}$, and $i = \{1, 2\}$. In the absence of any bias voltage or temperature gradient, as the asymmetry factors only enter in $\boldsymbol{W}^{\mathrm{eff}}$ through the tunneling rates, this results in similar relations when decomposing the effective kernel in its r-lead components, such that the same can be applied for the charge currents [cf. Eq. (18)],

$$\boldsymbol{W}_r^{\mathrm{eff}} = \frac{\Gamma_r}{\Gamma_{r'}}\boldsymbol{W}_{r'}^{\mathrm{eff}} \quad \Rightarrow \quad I_r^{(k)} = \frac{\Gamma_r}{\Gamma_{r'}} I_{r'}^{(k)}. \tag{C2}$$

On the other hand, charge conservation on the first order currents gives rise to the following relation

$$\sum_r I_r^{(1)} = -\frac{\mathrm{d}}{\mathrm{d}t}\left\langle \hat{n}\right\rangle^{(0)}, \tag{C3}$$

where $\hat{n}$ is the DQD occupation number operator. Hence, if we make use of Eq. (C2) we get

$$I_r^{(1)} = -\frac{\Gamma_r}{\Gamma}\frac{\mathrm{d}}{\mathrm{d}t}\left\langle \hat{n}\right\rangle^{(0)}. \tag{C4}$$

As the above quantity corresponds to a *total* time derivative of a periodic function, the pumped charge, defined as the time integral of $I_r^{(1)}$ over a period of the modulation cycle, clearly integrates to zero. This result is expected since no net charge can be accumulated/lost in the DQD system after each cycle.

---

[*] Corresponding author: rbustos@famaf.unc.edu.ar

[1] T. Brandes, "Coherent and collective quantum optical effects in mesoscopic systems," Phys. Rep. **408**, 315 – 474 (2005).

[2] N. A. Zimbovskaya, Transport Properties of Molecular Junctions (Springer, New York, NY, 2013).

[3] J. Wu and Z. M. Wang, Quantum Dot Molecules (Springer-Verlag, New York, USA, 2014).

[4] G. Benenti, G. Casati, K. Saito, and R. S. Whitney, "Fundamental aspects of steady-state conversion of heat to work at the nanoscale," Phys. Rep. **694**, 1–124 (2017).

[5] R. S. Whitney, R. Sánchez, and J. Splettstoesser, "Quantum thermodynamics of nanoscale thermoelectrics and electronic devices." in Thermodynamics in the Quantum Regime. Fundamental Theories of Physics, Vol. 195, edited by F. Binder, L. Correa, C. Gogolin, J. Anders, and G. Adesso (Springer, Cham, 2018).

[6] R. A. Bustos-Marún and H. L. Calvo, "Thermodynamics and steady state of quantum motors and pumps far from equilibrium," Entropy **21** (2019), 10.3390/e21090824.

[7] J. R. Prance, C. G. Smith, J. P. Griffiths, S. J. Chorley, D. Anderson, G. A. C. Jones, I. Farrer, and D. A. Ritchie, "Electronic refrigeration of a two-dimensional electron gas," Phys. Rev. Lett. **102**, 146602 (2009).

[8] M. Josefsson, A. Svilans, A. M. Burke, E. A. Hoffmann, S. Fahlvik, C. Thelander, M. Leijnse, and H. Linke, "A quantum-dot heat engine operating close to the thermodynamic efficiency limits," Nat. Nanotechnol. **13**, 920–924 (2018).

[9] C. W. J. Beenakker and A. A. M. Staring, "Theory of the thermopower of a quantum dot," Phys. Rev. B **46**, 9667–9676 (1992).

[10] F. Haupt, M. Leijnse, H. L. Calvo, L. Classen, J. Splettstoesser, and M. R. Wegewijs, "Heat, molecular vibrations, and adiabatic driving in non-equilibrium transport through interacting quantum dots," Phys. Status Solidi B **250**, 2315–2329 (2013).

[11] B. Sothmann, R. Sánchez, and A. N. Jordan, "Thermoelectric energy harvesting with quantum dots," Nanotechnology **26**, 032001 (2014).

[12] P. W. Brouwer, "Scattering approach to parametric pumping," Phys. Rev. B **58**, R10135 (1998).

[13] S. K. Watson, R. M. Potok, C. M. Marcus, and V. Umansky, "Experimental realization of a quantum spin pump," Phys. Rev. Lett. **91**, 258301 (2003).

[14] E. Cota, R. Aguado, and G. Platero, "ac-driven double quantum dots as spin pumps and spin filters," Phys. Rev. Lett. **94**, 107202 (2005).

[15] S. Juergens, F. Haupt, M. Moskalets, and J. Splettstoesser, "Thermoelectric performance of a driven double quantum dot," Phys. Rev. B **87**, 245423 (2013).

[16] C. A. Perroni, F. Romeo, A. Nocera, V. Marigliano Ramaglia, R. Citro, and V. Cataudella, "Noise-assisted charge pump in elastically deformable molecular junctions," J. Phys.: Condens. Matter **26**, 365301 (2014).

[17] M. Taguchi, S. Nakajima, T. Kubo, and Y. Tokura, "Quantum adiabatic pumping by modulating tunnel phase in quantum dots," J. Phys. Soc. Jpn. **85**, 084704 (2016).

[18] J. I. Romero, P. Roura-Bas, A. A. Aligia, and L. Arrachea, "Nonlinear charge and energy dynamics of an adiabatically driven interacting quantum dot," Phys. Rev. B **95**, 235117 (2017).

[19] P. Terrén Alonso, J. Romero, and L. Arrachea, "Work exchange, geometric magnetization, and fluctuation-dissipation relations in a quantum dot under adiabatic magnetoelectric driving," Phys. Rev. B **99**, 115424 (2019).

[20] L. M. Cangemi, V. Cataudella, G. Benenti, M. Sassetti, and G. De Filippis, "Violation of thermodynamics uncertainty relations in a periodically driven work-to-work converter from weak

to strong dissipation," Phys. Rev. B **102**, 165418 (2020).

[21] N. A. Zimbovskaya and A. Nitzan, "Energy, work, entropy, and heat balance in marcus molecular junctions," J. Phys. Chem. B **124**, 2632–2642 (2020).

[22] S. J. Chorley, J. Frake, C. G. Smith, G. A. C. Jones, and M. R. Buitelaar, "Quantized charge pumping through a carbon nanotube double quantum dot," App. Phys. Lett. **100**, 143104 (2012).

[23] B. Roche, R.-P. Riwar, B. Voisin, E. Dupont-Ferrier, R. Wacquez, M. Vinet, M. Sanquer, J. Splettstoesser, and X. Jehl, "A two-atom electron pump," Nat. Commun. **4**, 1581 (2013).

[24] A. Benyamini, A. Hamo, S. Viola Kusminskiy, F. von Oppen, and S. Ilani, "Real-space tailoring of the electron-phonon coupling in ultraclean nanotube mechanical resonators," Nat. Phys. **10**, 151 (2014).

[25] D. Dundas, E. J. McEniry, and T. N. Todorov, "Current-driven atomic waterwheels," Nat. Nanotechnol. **4**, 99 (2009).

[26] R. Bustos-Marún, G. Refael, and F. von Oppen, "Adiabatic quantum motors," Phys. Rev. Lett. **111**, 060802 (2013).

[27] L. J. Fernández-Alcázar, R. A. Bustos-Marún, and H. M. Pastawski, "Decoherence in current induced forces: Application to adiabatic quantum motors," Phys. Rev. B **92**, 075406 (2015).

[28] M. F. Ludovico, L. Arrachea, M. Moskalets, and D. Sánchez, "Periodic energy transport and entropy production in quantum electronics," Entropy **18** (2016), 10.3390/e18110419.

[29] A. Celestino, A. Croy, M. W. Beims, and A. Eisfeld, "Rotational directionality via symmetry-breaking in an electrostatic motor," New J. Phys. **18**, 063001 (2016).

[30] L. J. Fernández-Alcázar, H. M. Pastawski, and R. A. Bustos-Marún, "Dynamics and decoherence in nonideal Thouless quantum motors," Phys. Rev. B **95**, 155410 (2017).

[31] H. L. Calvo, F. D. Ribetto, and R. A. Bustos-Marún, "Real-time diagrammatic approach to current-induced forces: Application to quantum-dot based nanomotors," Phys. Rev. B **96**, 165309 (2017).

[32] A. Bruch, S. V. Kusminskiy, G. Refael, and F. von Oppen, "Interacting adiabatic quantum motor," Phys. Rev. B **97**, 195411 (2018).

[33] M. Hopjan, G. Stefanucci, E. Perfetto, and C. Verdozzi, "Molecular junctions and molecular motors: Including coulomb repulsion in electronic friction using nonequilibrium green's functions," Phys. Rev. B **98**, 041405(R) (2018).

[34] M. F. Ludovico and M. Capone, "Enhanced performance of a quantum-dot-based nanomotor due to coulomb interactions," Phys. Rev. B **98**, 235409 (2018).

[35] H. H. Lin, A. Croy, R. Gutierrez, C. Joachim, and G. Cuniberti, "Current-induced rotations of molecular gears," J. Phys. Commun **3**, 025011 (2019).

[36] L. J. Fernández-Alcázar, H. M. Pastawski, and R. A. Bustos-Marún, "Nonequilibrium current-induced forces caused by quantum localization: Anderson adiabatic quantum motors," Phys. Rev. B **99**, 045403 (2019).

[37] P. Qin and H. C. Park, "Electronic current in a nano-mechanical kicked electron shuttle," Physica E: Low Dimens. Syst. Nanostruct. **117**, 113835 (2020).

[38] M. F. Ludovico, F. Battista, F. von Oppen, and L. Arrachea, "Adiabatic response and quantum thermoelectrics for ac-driven quantum systems," Phys. Rev. B **93**, 075136 (2016).

[39] J. E. Avron, A. Elgart, G. M. Graf, and L. Sadun, "Transport and dissipation in quantum pumps," J. Stat. Phys. **116**, 425 (2004).

[40] D. Cohen, T. Kottos, and H. Schanz, "Quantum pumping: The charge transported due to a translation of a scatterer," Phys. Rev. E **71**, 035202(R) (2005).

[41] K. Brandner, "Coherent transport in periodically driven mesoscopic conductors: From scattering amplitudes to quantum thermodynamics," Z. Naturforsch. A **75**, 483 – 500 (2020).

[42] J. Splettstoesser, M. Governale, J. König, and R. Fazio, "Adiabatic pumping through a quantum dot with Coulomb interactions: A perturbation expansion in the tunnel coupling," Phys. Rev. B **74**, 085305 (2006).

[43] N. Winkler, M. Governale, and J. König, "Diagrammatic real-time approach to adiabatic pumping through metallic single-electron devices," Phys. Rev. B **79**, 235309 (2009).

[44] F. Cavaliere, M. Governale, and J. König, "Nonadiabatic pumping through interacting quantum dots," Phys. Rev. Lett. **103**, 136801 (2009).

[45] H. L. Calvo, L. Classen, J. Splettstoesser, and M. R. Wegewijs, "Interaction-induced charge and spin pumping through a quantum dot at finite bias," Phys. Rev. B **86**, 245308 (2012).

[46] R. I. Shekhter, L. Y. Gorelik, M. Jonson, Y. M. Galperin, and V. M. Vinokur, "Nanomechanical shuttle transfer of electrons," J. Comput. Theor. Nanosci. **4**, 860–895 (2007).

[47] A. R. Hernández, F. A. Pinheiro, C. H. Lewenkopf, and E. R. Mucciolo, "Adiabatic charge pumping through quantum dots in the coulomb blockade regime," Phys. Rev. B **80**, 115311 (2009).

[48] F. Deus, A. R. Hernández, and M. A. Continentino, "Adiabatic charge and spin pumping through interacting quantum dots," J. Phys. Condens. Matter **24**, 356001 (2012).

[49] R.-P. Riwar and J. Splettstoesser, "Charge and spin pumping through a double quantum dot," Phys. Rev. B **82**, 205308 (2010).

[50] B. Hiltscher, M. Governale, and J. König, "Interference and interaction effects in adiabatic pumping through quantum dots," Phys. Rev. B **81**, 085302 (2010).

[51] N. Bode, S. V. Kusminskiy, R. Egger, and F. von Oppen, "Scattering theory of current-induced forces in mesoscopic systems," Phys. Rev. Lett. **107**, 036804 (2011).

[52] B. Cunningham, T. N. Todorov, and D. Dundas, "Nonconservative current-driven dynamics: beyond the nanoscale," Beilstein J. Nanotechnol. **6**, 2140–2147 (2015).

[53] L. Gu and H.-H. Fu, "Current-induced enhancement of DNA bubble creation," New J. Phys **18**, 053032 (2016).

[54] M. Bai, C. S. Cucinotta, Z. Jiang, H. Wang, Y. Wang, I. Rungger, S. Sanvito, and S. Hou, "Current-induced phonon renormalization in molecular junctions," Phys. Rev. B **94**, 035411 (2016).

[55] J.-T. Lü, B.-Z. Hu, P. Hedegård, and M. Brandbyge, "Semi-classical generalized langevin equation for equilibrium and nonequilibrium molecular dynamics simulation," Prog. Surf. Sci. **94**, 21–40 (2019).

[56] F. Chen, K. Miwa, and M. Galperin, "Current-induced forces for nonadiabatic molecular dynamics," J. Phys. Chem. A **123**, 693–701 (2019).

[57] J. König, J. Schmid, H. Schoeller, and G. Schön, "Resonant tunneling through ultrasmall quantum dots: Zero-bias anomalies, magnetic-field dependence, and boson-assisted transport," Phys. Rev. B **54**, 16820 (1996).

[58] J.-T. Lü, M. Brandbyge, and P. Hedegård, "Blowing the fuse: Berry's phase and runaway vibrations in molecular conductors," Nano Lett. **10**, 1657–1663 (2010).

[59] T. Pluecker, M. R. Wegewijs, and J. Splettstoesser, "Gauge freedom in observables and landsberg's nonadiabatic geometric phase: Pumping spectroscopy of interacting open quantum systems," Phys. Rev. B **95**, 155431 (2017).

[60] D.J. Thouless, "Quantization of particle transport," Phys. Rev. B **27**, 6083 (1983).

[61] B. Bhandari, P. T. Alonso, F. Taddei, F. von Oppen, R. Fazio, and L. Arrachea, "Geometric properties of adiabatic quantum thermal machines," Phys. Rev. B **102**, 155407 (2020).

[62] H.-A. Engel and D. Loss, "Single-spin dynamics and decoherence in a quantum dot via charge transport," Phys. Rev. B **65**, 195321 (2002).

[63] It is straightforward to include in the model of decoherence also a thermalization mechanism. However, for the particular example used here, this effect does not have any impact on the system as we are in the limit of degenerate quantum levels.

[64] B. Wunsch, M. Braun, J. König, and D. Pfannkuche, "Probing level renormalization by sequential transport through double quantum dots," Phys. Rev. B **72**, 205319 (2005).

[65] M. Leijnse and M. R. Wegewijs, "Kinetic equations for transport through single-molecule transistors," Phys. Rev. B **78**, 235424 (2008).